Nano Energy 123 (2024) 109407

Contents lists available at ScienceDirect

Nano Energy

journal homepage: www.elsevier.com/locate/nanoen

Full paper

Stretchable electronic facial masks for photodynamic therapy

Lijuan Zhang [a,1], Xiaoxiao Jiang [b,c,1], Shuang Li [a,d], Yuqun Lan [a,d], Hao Liu [a,e], Haiying Yu [f], Aochen Wang [a], Maoyi Zhang [a,d,g], Juyao Li [a,d], Guodong Liu [a,d], Guangping Gong [h], Mingqi Huang [h], Qinlan Li [a,d], Yang Zhao [a,d], Kun Zhu [f], Liang Guo [a], Li Duan [d,i], Yuli Chen [e], Bo Wang [h], Rui Li [h,*], Ya Yang [g,j,**], Yewang Su [a,d,***]

[a] State Key Laboratory of Nonlinear Mechanics, Institute of Mechanics, Chinese Academy of Sciences, Beijing 100190, China
[b] Key Laboratory of Animal Ecology and Conservation Biology, Institute of Zoology, Chinese Academy of Sciences, Beijing 100101, China
[c] College of Life Science, University of Chinese Academy of Sciences, Beijing 100049, China
[d] School of Engineering Science, University of Chinese Academy of Sciences, Beijing 100049, China
[e] Institute of Solid Mechanics, Beihang University (BUAA), Beijing 100191, China
[f] CAS Key Laboratory of Microbial Physiological and Metabolic Engineering, Institute of Microbiology, Chinese Academy of Sciences, Beijing 100101, China
[g] CAS Center for Excellence in Nanoscience, Beijing Key Laboratory of Micro-Nano Energy and Sensor, Beijing Institute of Nanoenergy and Nanosystems, Chinese Academy of Sciences, Beijing 101400, China
[h] State Key Laboratory of Structural Analysis, Optimization and CAE Software for Industrial Equipment, Department of Engineering Mechanics, and International Research Center for Computational Mechanics, Dalian University of Technology, Dalian 116024, China
[i] Key Laboratory of Microgravity, Institute of Mechanics, Chinese Academy of Sciences, Beijing 100190, China
[j] School of Nanoscience and Technology, University of Chinese Academy of Sciences, Beijing 100049, China

ARTICLE INFO

Keywords:
Facial mask
Stretchable electronics
Photodynamic therapy
Skin care

ABSTRACT

In this paper, we introduce a novel stretchable electronic facial mask for photodynamic therapy (SEFMPT) integrated with red-blue-green LED arrays, which realizes several favorable characteristics such as portability, uniformity of illuminance on the human face, and hands-free for personal long-time use. To achieve high mechanical, thermal and electrical performances of the SEFMPT, an unusual design of thick multilayer organic-inorganic composite (TMOIC) serpentine interconnects and a new piecewise single-side soft pressing (PSSP) technique for encapsulation are developed, which could also be extended to the design and fabrication of other stretchable electronics. By integrating the tri-color LEDs that could independently irradiate red, blue, and green lights, the multifunctional therapeutic purpose is realized, including skin anti-aging, treatment of Propionibacterium acnes (P. acnes) and skin whitening. The exploitation of the SEFMPT provides a distinct opportunity for new developments in both photodynamic technology and wearable electronics.

1. Introduction

Photodynamic technology has been widely recognized as an effective non-invasive method for therapeutic use [1–6]. Specifically, red light is effective in controlling the pain and reducing the time of wound healing by stimulating collagen production, fibroblast proliferation and local microvasculature as well as by stimulating cellular metabolism to enhance tissue regeneration [7–9]. Blue light could be used for antiphlogosis by inactivating *Propionibacterium acnes* (*P. acnes*), which is a kind of bacteria that causes pustules on the skin surface. Combined with the 5-aminolevulinic acid (5-ALA) photosensitizer, the inactivation effect of blue light could be further promoted [10–13]. Green light plays an important role in skin whitening. From the viewpoint of the biological mechanism, melanin deposition causes darkening of the skin, while the green light could inhibit the activity of the tyrosinase, which is the rate-limiting factor for biosynthesis of melanin, and could thus take

* Corresponding author.
** Corresponding author at: CAS Center for Excellence in Nanoscience, Beijing Key Laboratory of Micro-Nano Energy and Sensor, Beijing Institute of Nanoenergy and Nanosystems, Chinese Academy of Sciences, Beijing 101400, China.
*** Corresponding author at: State Key Laboratory of Nonlinear Mechanics, Institute of Mechanics, Chinese Academy of Sciences, Beijing 100190, China.
E-mail addresses: ruili@dlut.edu.cn (R. Li), yayang@binn.cas.cn (Y. Yang), yewangsu@imech.ac.cn (Y. Su).
[1] These authors contributed equally to this work.

https://doi.org/10.1016/j.nanoen.2024.109407
Received 1 January 2024; Received in revised form 6 February 2024; Accepted 16 February 2024
Available online 17 February 2024

effect for skin whitening [14–16].

Since improving facial health conditions is of great significance for people of all ages [17–21], it may be a promising idea to develop a wearable electronic device based on the technique of photodynamic therapy for facial healthcare. As we know, some rigid-platform cabinet-type electronic devices have been used in hospitals or beauty institutions for promoting wound healing or improving skin condition by photodynamic therapy, but the user will stay in designated locations for treatment, because these devices require a fixed space and location to accommodate a console (power supply) attached to the applicator (light deliverer) via a cable [22,23]. Therefore, the portability of the equipment is necessary for wider applications. In recent years, a variety of hand-held and hard masked photodynamic therapy devices are accepted for facial healthcare, which have smaller size, lighter weight and portability. However, the most hand-held devices could not irradiate the full face; meanwhile, it is hard to realize hand-free during use. And the hard mask style devices consist of a hard shell, circuit and LED light, which has a certain weight, for which it is not suitable for long-time wear. In view of the above situation, it is possible to introduce the flexible electronic technology into the design of photodynamic therapy devices to obtain light weight, flexible, even stretchable photodynamic electronic masks. However, there have been rare reports on the development of such a fascinating device in previous studies. The primary reason is that several inevitable requirements and challenges in the design strategy must be well addressed. **(1) Portability.** The increasing demand for portability is that the device has light weight, compact size, and the ability to be folded or rolled up; meanwhile, the common power bank is used as the power supply for the device working well, such that the complete set of the device could be carried in a handbag and is usable whenever and wherever possible. **(2) Uniformity of illuminance on the human face.** While serving as the most concerned part of skin treatment, the human face constitutes the most complicated undevelopable surface of the human body. Accordingly, a relatively large-area and uniform irradiation from the device is necessary for an effective photodynamic therapy, which could not be realized by conventional devices [24]. **(3) Hands-free for personal long-time use.** The device

Fig. 1. Display and mechanism of the SEFMPT. a) Appearance and the way of wearing of the SEFMPT. b) Independent control of tri-color lights. c) Apparent view of the SEFMPT, including a top silicone encapsulation layer (1), a layer of stretchable island-bridge mesh structure with an array of LEDs (2), and a bottom silicone encapsulation layer (3). d) Key stretchable island-bridge mesh structure of the SEFMPT, with e) a locally enlarged view of each layer. f) Schematic of the underlying mechanism of tri-color lights therapy.

should be made for hands-free operation such that the hands are available for other jobs during the use of the device. This requirement obviously distinguishes the device from the existing hand-held ones [25–27] such that a multi-task mode is accomplished. However, it is obviously a quite challenging job to simultaneously address the above three favorable aspects in one device.

In this paper, we introduce a novel stretchable electronic facial mask for photodynamic therapy (SEFMPT) that could address all above requirements and challenges. It is actually a platform of photodynamic therapy for the human face, on which sensors for water content, elasticity, roughness, etc. could be integrated. As a demonstration, photodynamic functional components (red-blue-green LED arrays) are integrated into the platform for wound healing, antiphlogosis and skin whitening. To achieve high mechanical, thermal and electrical performances of the SEFMPT, the unusual design of thick multilayer organic-inorganic composite (TMOIC) serpentine interconnects and the new piecewise single-side soft pressing (PSSP) technique for encapsulation are developed, which could also be applied to other stretchable electronics. The collective results show great potential of the SEFMPT for skin therapy. The exploitation of the present device provides a distinct opportunity for new developments in both photodynamic technology and wearable electronics.

2. Results and discussion

2.1. Display and mechanism of the SEFMPT

The appearance and the way of wearing the SEFMPT are the same as those of conventional facial masks, as shown in Fig. 1a. Three different colors of lights could be controlled independently, as shown in the video 1 (Fig. 1b). As shown in Fig. 1c, the SEFMPT is composed of three layers, including a layer of stretchable island-bridge mesh structure with an array of LEDs (layer 2) and two silicone encapsulation layers positioned at the top (layer 1) and bottom (layer 3). The inner silicone encapsulation layer near the LED array and the human face (layer 1) is transparent such that the light from the LEDs could irradiate the face. The outer silicone encapsulation layer (layer 3) is white such that the received light could be reflected to the skin. Using soft and transparent glue, of which the elastic modulus is much lower than that of silicone, the three layers are bonded together. The stretchable island-bridge mesh structure of a SEFMPT is schematically illustrated in Fig. 1d, with a locally enlarged view of the details shown in Fig. 1e. The structure is composed of four layers of Cu as conductive layers and five layers of polyimide (PI) as insulative and packaging layers, besides the integrated LEDs. The circuit of a SEFMPT is designed to have 386 islands, i.e., the same number of LEDs are integrated. To ensure that the skin of the face is fully irradiated with the light from the LED array at a very close distance (~2 mm), the layout of the LEDs is specially designed. As shown in Figure S1 in the Supporting Information, the LEDs in the array are arranged annularly by fixing the horizontal and vertical spacing between two adjacent islands. In this case, the skin could be fully covered when the irradiation distance is longer than 2.33 mm. With the increase of irradiation distance, the light density exhibits better uniformity.

Supplementary material related to this article can be found online at doi:10.1016/j.nanoen.2024.109407.

Fig. 1f illustrates the underlying mechanism of skin protection by the tri-color SEFMPT. Basically, the red light works on deep dermal cells. The physiological dose could activate small GTPase Ras, Raf, phosphorylated ERK pathway. The calcium pool would be triggered when the red light acts on the endoplasmic reticulum, and ERK would then be activated. The phosphorylated ERK could be transported to cell nucleus and interact with different kinds of transcription factors (such as SP1, ATF, EIK-1, and NF-kB), which finally promotes cell proliferation and migration on wound bed [28–31]. The blue light and exogenous alanine co-work on sebocytes and promote the synthesis of porphyrins, further destroying the bacterial structure through photodynamic action to cause bacterial death and control inflammation [21,32,33]. The green light works on melanophores to inhibit the activity of tyrosinase that promotes tyrosine -> DOPA -> dopaquinone generation, and reduces melanogenesis finally [14,16,34].

2.2. Fabrication of the SEFMPT

The stretchable island-bridge mesh structure integrated with an array of tri-color LEDs is the key portion of the SEFMPT, of which the fabrication process is outlined in Fig. 2a. The starting substrates included two pieces of double-sided flexible Cu-clad laminates: one with the 55-μm-thick Cu-1 layer and 35-μm-thick Cu-2 layer, and another with 35-μm-thick Cu-3 layer and 55-μm-thick Cu-4 layer, double-sided flexible Cu-clad laminates had a 25-μm-thick supporting PI layer in between double-sided Cu. The fabrication initially began with patterning 140-μm-wide Cu meanders, island-like bonding pads and openings by photolithography and wet etching along with the standard design for Cu-1, Cu-2, Cu-3 and Cu-4 (see Fig. 1e). A 50-μm-thick PI layer was then sandwiched between the two patterned substrates. The bonding pads of anode and tri-color light were fabricated on Cu-1 layer. The through-holes were made by the technology of punching and Cu deposition in the edge of the through-holes, which connected three bonding pads of anode, blue light, and green light of a LED, respectively, to realize transmission of the current through the multilayer electronic circuit board. The PI supporting layers had three small punching holes in the island for current transmission between the upper and lower layers. The small openings in the Cu layers were for current output in these layers, but the bigger openings in the same layers were not for the current output in these layers, just allowed the current passing to the next layer. The current flow is schematically shown in Figure S2. Taking an island structure as an example, the current input is from Cu-4, which directly flows into the anode of the LED light on Cu-1. Cu-1, Cu-2 and Cu-3 serve as the current output layers that correspond to red, blue, and green lights, respectively. The multilayer design of the layout makes the tri-color LEDs controllable independently. Then, a 50-μm-thick PI sheet was laminated at the bottom of the integration (i.e., on the Cu-4 layer) as a cover film, and another 50-μm-thick PI layer that was hollowed out in the location corresponding to the bonding pads was laminated on the Cu-1 layer. The island-bridge-like layout was structured in one step by laser cutting, and then the flexible circuit board residues were removed by peeling them off. The width of PI in stretchable interconnects was 340 μm, which was larger than that of Cu meanders for protection of the latter against mechanical failure under stretching [35–37]. By assembling the tri-color LEDs (type 1516, with length: 1.6 mm, width: 1.5 mm, and height: 0.6 mm) on the “islands”, fabrication of the stretchable island-bridge mesh structure integrated with an array of tri-color LEDs was finalized.

A great challenge next is the encapsulation of the above-generated mesh structure with a bumpy morphology. On the one hand, a conformable fit to the human face that has a complicated undevelopable surface requires that the encapsulated device should have a soft geometry. That is, a low stiffness of the SEFMPT must be guaranteed. On the other hand, effective photodynamic therapy requires that a uniform illuminance on the entire human face should be realized, for which an encapsulation strategy incorporating every part of the human face is necessary. To address the above major concerns, a novel PSSP technique is exploited in this study, as elaborated in the following.

Fig. 2b shows the way of partition of an entire SEFMPT toward the PSSP for encapsulation. The complicated SEFMPT (Fig. 2b, left) is divided into five portions approaching planar configurations (Fig. 2b, middle), which correspond to five steel plates (Fig. 2b, right) that will be used later. Fig. 2c illustrates the PSSP toward large flexibility of the SEFMPT, which requires that the adhesive layer between the inner and outer silicone layers is thin enough since adhesive has unfavorable large stiffness when solidified. Here, the island-bridge mesh structure is sandwiched by the two silicone layers, with the bumpy morphology

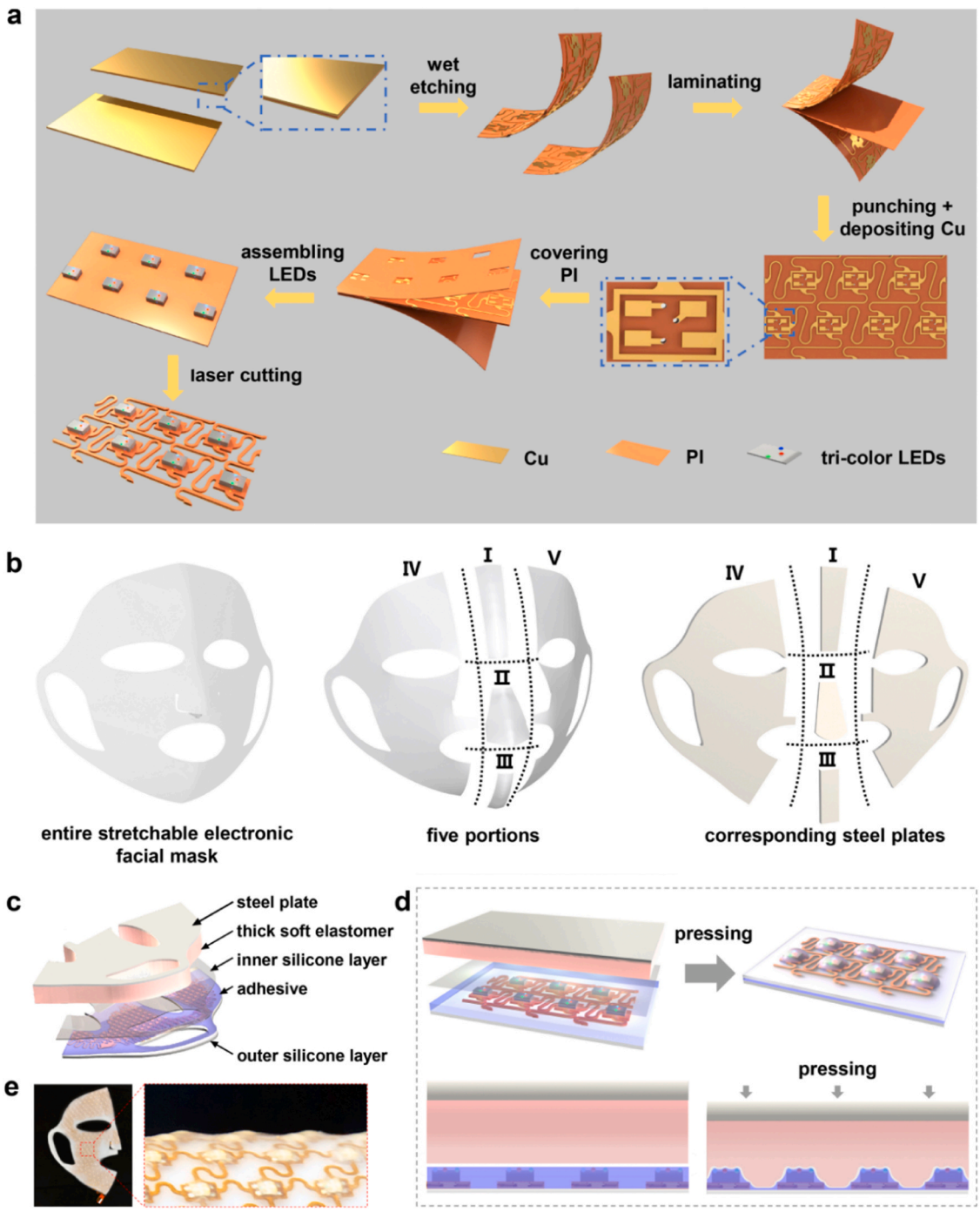

Fig. 2. Fabrication of the SEFMPT. a) Fabrication process of the SEFMPT before encapsulation. b) Partition of an entire SEFMPT toward the PSSP for encapsulation. c) Expanded view and d) views of the PSSP process. e) SEFMPT after the PSSP.

filled up with liquid adhesive (K-705, Kafuter, China). The inner silicone layer side is covered by a thick soft elastomer (with thickness of 8 mm and Young's modulus of 60 kPa), and then a rigid steel plate (with thickness of 3 mm and Young's modulus of 210 GPa). Accordingly, from top to bottom, we have the steel plate, thick soft elastomer, inner silicone layer, island-bridge mesh structure with liquid adhesive, and outer silicone layer, respectively. Fig. 2d illustrates the PSSP process. Pressing the steel plate downward with an appropriate force (~ 100 N) and keeping still until solidification of the adhesive, the encapsulation is realized. With the aid of the thick soft elastomer, the island-bridge mesh structure is enveloped by the inner silicone layer due to pressure. Much of the liquid adhesive is squeezed out of the edge of the SEFMPT and then cleaned up. The solidified adhesive ensures an effective bond of the two silicone layers, with the bumpy island-bridge mesh structure firmly sandwiched in between (Fig. 2e). The practical encapsulation for the two half faces is achieved one by one. The weight of a finished SEFMPT is ~ 48.9 g. For a face area of ~ 20 cm × 20 cm, the pressure caused by the weight only (without consideration of the tension of the SEFMPT) is as small as ~ 12.2 Pa such that a user would not feel uncomfortable.

2.3. *Mechanical, thermal and electrical performances of the SEFMPT*

There is no doubt that high mechanical, thermal and electrical performances should be realized for the SEFMPT. On the one hand, the

device needs robust mechanical stretchability for intimate conformability with the human face. On the other hand, a low electrical resistance could avoid excessive heat generation, which may cause premature failure of the device. It has been revealed in the previous studies that a thick PI layer may help increase the ductility of a thin Cu layer by delocalizing its deformation, enhancing the restoring ability and antifatigue ability [35,36,38–40]. However, to ensure the electrical performance of the SEFMPT, Cu layers must be thick enough. To address the above challenge, in the following, we present a novel TMOIC design for serpentine interconnects of the SEFMPT, with a thickness of tens of microns for a metal layer. The superior mechanical, thermal and electrical performances are elaborated in the following.

It is first verified that the SEFMPT could withstand relatively large deformation, which may be stretched (Fig. 3a), bent (Fig. 3b) and twisted (Fig. 3c), enabling conformable application to the human face for treating skin issues and improving skin conditions. The exceptional mechanical performance is mainly credited to the Cu-PI TMOIC structure. To validate the protective effect of PI against rupture of Cu in a quantitative way, we conducted the uniaxial tensile tests for a single layer of 18-μm-thick Cu with a straight-line geometry as well as a 50/55/25/35/50/35/25/55/50-μm-thick PI/Cu/PI/Cu/PI/Cu/PI/Cu/PI multilayered structure with the same geometry under the same length (6 mm) and width (0.14 mm). The curves of tensile force versus the applied strain in Fig. 3d show that the failure strain of the Cu-PI composite structure (>25%) is much larger than that of a single layer of Cu (~1.5%), and thus the former could provide robust stretchability. In addition to utilizing the TMOIC structure, the geometric layouts are designed to further enhance the stretchability. The finite element analysis (FEA) in Fig. 3e confirms that the maximum principal strains (<2.5%, blue area of the color bar) of the serpentine interconnects made of such a composite structure in the SEFMPT are far below its ductility (>25%) when the device is uniaxially stretched to 100% and 90% applied strains horizontally and vertically, respectively. The applied strains are different in two directions due to different distances between adjacent LEDs. The tensile stiffness of the island-bridge mesh structure with encapsulation is defined as the tensile force divided by the applied strain. Fig. 3f plots the relative tensile stiffnesses of the device to human skin (Young's modulus = 600 kPa and thickness = 1.5 mm) [41] in uniaxial horizontal and vertical stretching (Note S1, Supporting Information). Figure S3 shows the reaction force per unit divided by tensile stiffnesses per unit width of human skin as a function of the applied strain. As the applied strain increases, the cross-sectional area of the

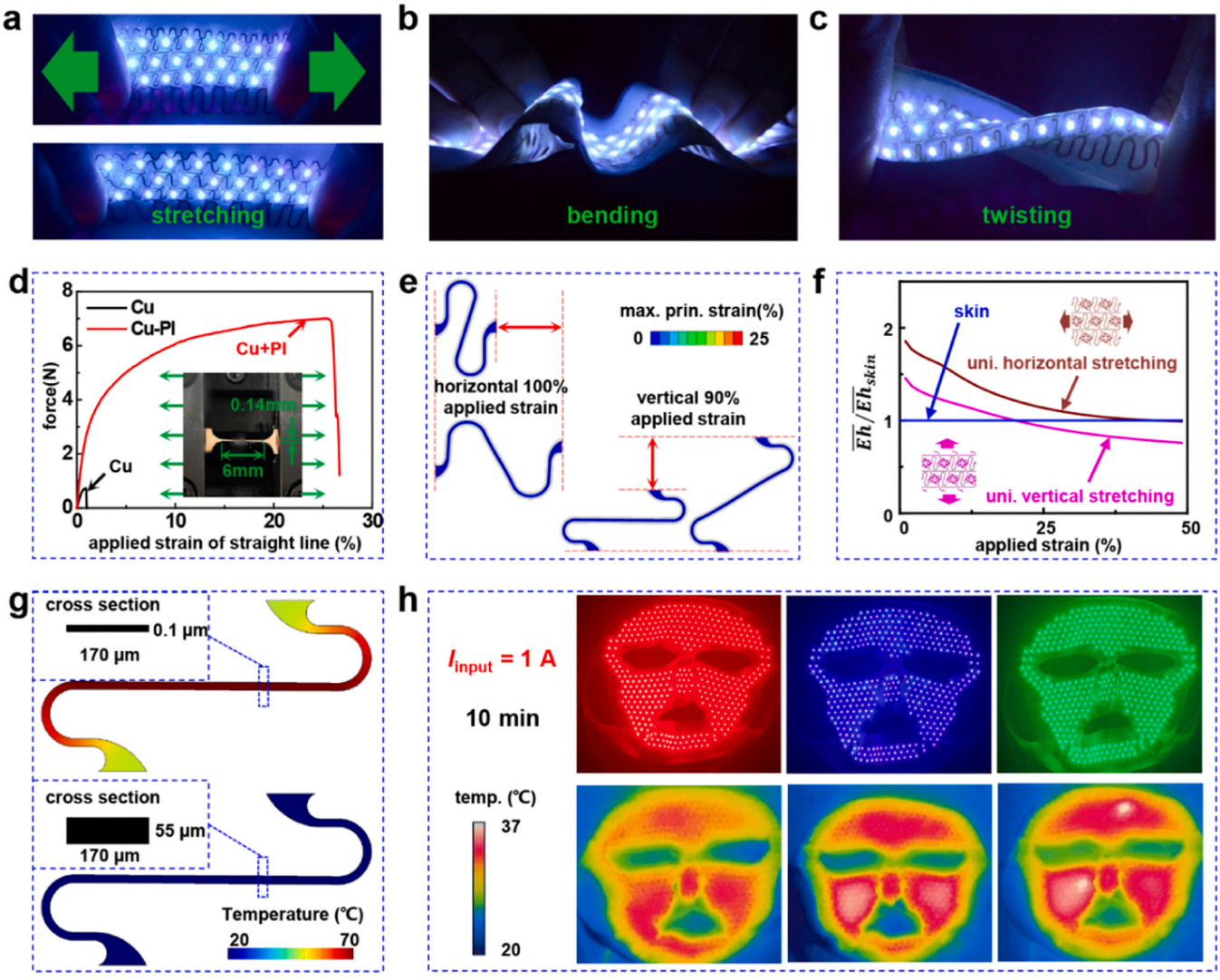

Fig. 3. Large deformation of the SEFMPT. a) stretching, b) bending, and c) twisting. d) Force-applied strain curves of a single Cu layer and a Cu-PI composite. e) Strain distribution in the Cu-PI composite structure when uniaxially stretched to 100% and 90% applied strains horizontally and vertically. f) Relative tensile stiffnesses of the device to human skin in uniaxial horizontal and vertical stretching. g) Temperature distribution in typical serpentine Cu interconnects with two different cross-section dimensions. h) Temperature distribution in the SEFMPT with a 10 min input of 1 A electric current under the ambient temperature of 20 °C.

encapsulation layers decreases, resulting in a decrease in the tensile stiffnesses. Under relatively large applied strain (>38%), the stiffnesses of the device in both directions could be even lower than that of the skin, which demonstrates satisfactory flexibility of the device.

Fig. 3g illustrates the temperature distribution obtained by thermal-electrical modeling in typical serpentine Cu interconnects with two different cross-section dimensions (Note S2, Supporting Information). With a 10 mA electric current applied under the ambient temperature of 20 °C, the 55-μm-thick interconnect provides a nearly uniform distribution of very low temperature (20.08 °C), while the 0.1-μm-thick interconnect yields a non-uniform distribution of significantly higher temperature, which could reach as high as 73.85 °C. Compared with ~ 0.1-μm-thick ultra-thin interconnect as adopted in many previous studies [42,43], a relatively thick interconnect (e.g., with 55 μm thickness) could obviously achieve very low electrical resistance and heat generation, which is highly favorable for applications in high-power wearable electronics. Accordingly, such a thick interconnect layout has been used for the present SEFMPT. Specifically, with a 10 min input of 1A electric current under the ambient temperature of 20 °C, the temperature in a tri-color SEFMPT does not exceed the human body temperature (37 °C), as revealed by the infrared thermograms shown in Fig. 3h (FLIR T420, FLIR Systems, USA), which implies that there are no thermal comfort problems when using the present device.

According to the volt-ampere characteristics of the LED array (Figure S4a, Supporting Information), the intensities of the currents passing different lights of LEDs are different. A slight change of voltage caused by the resistance of Cu interconnects may bring a significant change of electric current, which impacts the luminance of the LEDs, especially the ones far away from the connection port. Therefore, it is necessary to control the resistance of the interconnects. The equivalent resistance of the red lights is the minimum among the three lights when the input current is 9 mA according to the volt-ampere characteristics (Figure S4b, Supporting Information). The current flows through 17 islands and bridges, and the resistance of the interconnects between the connection port and the far end should be less than 0.64 Ω. Therefore, the resistance of a single island and bridge should be less than 37.65 mΩ. Accordingly, the resistance of a single island is estimated to be 4.375 mΩ, by which we obtain the maximum resistance of a single bridge to be 33.275 mΩ, ensuring relatively uniform irradiation (Details appear in the Experimental Section). Figure S5 in the Supporting Information shows the simulated voltage distribution in two units of the serpentine interconnects, which is obtained by the COMSOL software package (Note S3, Supporting Information). The Electric Currents interface is chosen in AC/DC module of the COMSOL software to conduct the stationary analysis. Ground and terminal boundaries are prescribed in the physical field, where the terminal current is 1 A. According to the simulation results, the resistances of the horizontal and vertical interconnects are 33.0 and 30.8 mΩ, respectively. Based on our measurement, the resistance of a single interconnect is lower than 33.275 mΩ; this value meets the requirement of resistance control for application to the SEFMPT (Details appear in the Experimental Section).

2.4. Effects of tri-color light irradiation by the SEFMPT on skin care

As an effective means of non-invasive treatment, the application value of photodynamic therapy has been fully demonstrated in the field of skin care. It has also been revealed that different wavelengths of light shining on the skin could effectively treat different skin problems. Accordingly, for the present SEFMPT with the tri-color light irradiation to realize multifunctional therapeutic purposes, the specific effects on skin care are examined. Dermal cells' activity is crucial for promoting collagen fiber synthesis, and thus is of fundamental importance for elasticity and shine of the skin. Due to its strong tissue penetration and remarkable effect on increasing cellular activity, the red light with 620 ± 20 nm wavelength has been selected for achieving skin elasticity and shine [30,31]. To confirm the effectiveness of the above light, human skin fibroblasts (HSFs) were irradiated with the light from the SEFMPT (Figure S6a, Supporting Information), followed by the MTT test to measure the cell activity. As shown in Fig. 4a, the activity of HSFs that were irradiated for 40 and 60 min is much higher than the nonirradiated control group. Meanwhile, after 40 min exposure, the phosphorylation of extracellular signal-regulated kinase (ERK), as an essential course for initiating cell proliferation, was dramatically increased in the same treated group (Fig. 4b). To further confirmed the effect of promoting cell proliferation of the SEFMPT, FACS analysis was used to classify cell cycle. We found that the percentage of cells in G0/G1-phase reduced about 6% whereas it increased in S-phase after irradiated with the light, suggesting that red light from SEFMPT promoted the transition of G0/G1- to S-phase, demonstrated an increase in cell proliferation (Fig. 4c). Fibroblasts migration is a key co-event during acne repair and is also under ERK pathway regulation [44]. To verify this, the cell scratch assay was conducted and the results showed that many more HSFs migrated to the blank area caused by scratch after SEFMPT treatment compared with the non-treated group (Fig. 4d).

P. acnes is a key acne vulgaris-inducing bacterium, which could induce de novo synthesis of porphyrins by using aminolevulinic acid (ALA). Blue light irradiation could kill the bacterium by inducing a reactive oxygen species (ROS) burst [12,13]. Theoretically, combined with 5-ALA (working as the ALA donor), blue light could suppress *P. acnes* that infects the skin and thus could well treat acne vulgaris, for which *P. acnes* was irradiated with the blue light from the SEFMPT (Figure S6b, Supporting Information). As shown in Fig. 4e, almost all *P. acnes* were killed by blue light treatment when the initial cfu of *P. acnes* was 10^4. 1 g/L of 5-ALA was able to suppress more than 80% of the bacterium under coprocessing of the blue light and the survival rate of *P. acnes* was negatively correlated with the 5-ALA co-incubation concentration when the initial cfu of *P. acnes* was less than 10^5 (Fig. 4f). Increasing the initial cfu of *P. acnes* to 10^6, the combined effect of blue light and 5-ALA on suppressing *P. acnes* was still significant (Fig. 4g), while the *P. acnes* survival impairment function was diminished when the natural light was applied instead of the blue light, even though the 5-ALA incubation concentration was increased (grey bars). Similarly, when 5-ALA was deprived, the blue light alone could not reduce the number of *P. acnes*, indicating that 5-ALA is essential for treating acne. On the other hand, the effect of the blue light and 5-ALA on *P. acnes* survival suppression was overwhelmed when the initial cfu reached 10^7 (Fig. 4h).

The green light with 525 ± 20 nm wavelength was designed for skin whitening via reducing melanin content in melanocytes. To confirm the effectiveness of the above light, melanocytes were irradiated and the total melanin in each group was extracted and measured (Figure S6c, Supporting Information). The results showed a significant reduction in the relative melanin level in 40- and 60-min irradiation groups (Fig. 4i). The following MTT test results indicated that the green light could not change the proliferation rate of melanocytes (Fig. 4j). These results demonstrated that the green light from the SEFMPT could lower the melanin content but was independent of reducing melanocytes counts. It is well known that tyrosinase is the rate-limiting factor for biosynthesis of melanin [16]. Our further data showed that the very dose of green light we used in previous experiments effectively inhibited the activity of tyrosinase (Fig. 4k) but did not influence its expression (Fig. 4l), revealing that the green light we used could reduce the biosynthesis of melanin.

3. Conclusion

Motivated by the high demand for developing portable active therapeutic tools for skin care of the human face, which was rarely reported in previous studies, here we introduce a novel SEFMPT. Taking advantage of the functions of red, blue, and green lights, the independently controlled tri-color LEDs are integrated into highly stretchable platforms for wound healing, antiphlogosis and skin whitening. The extreme

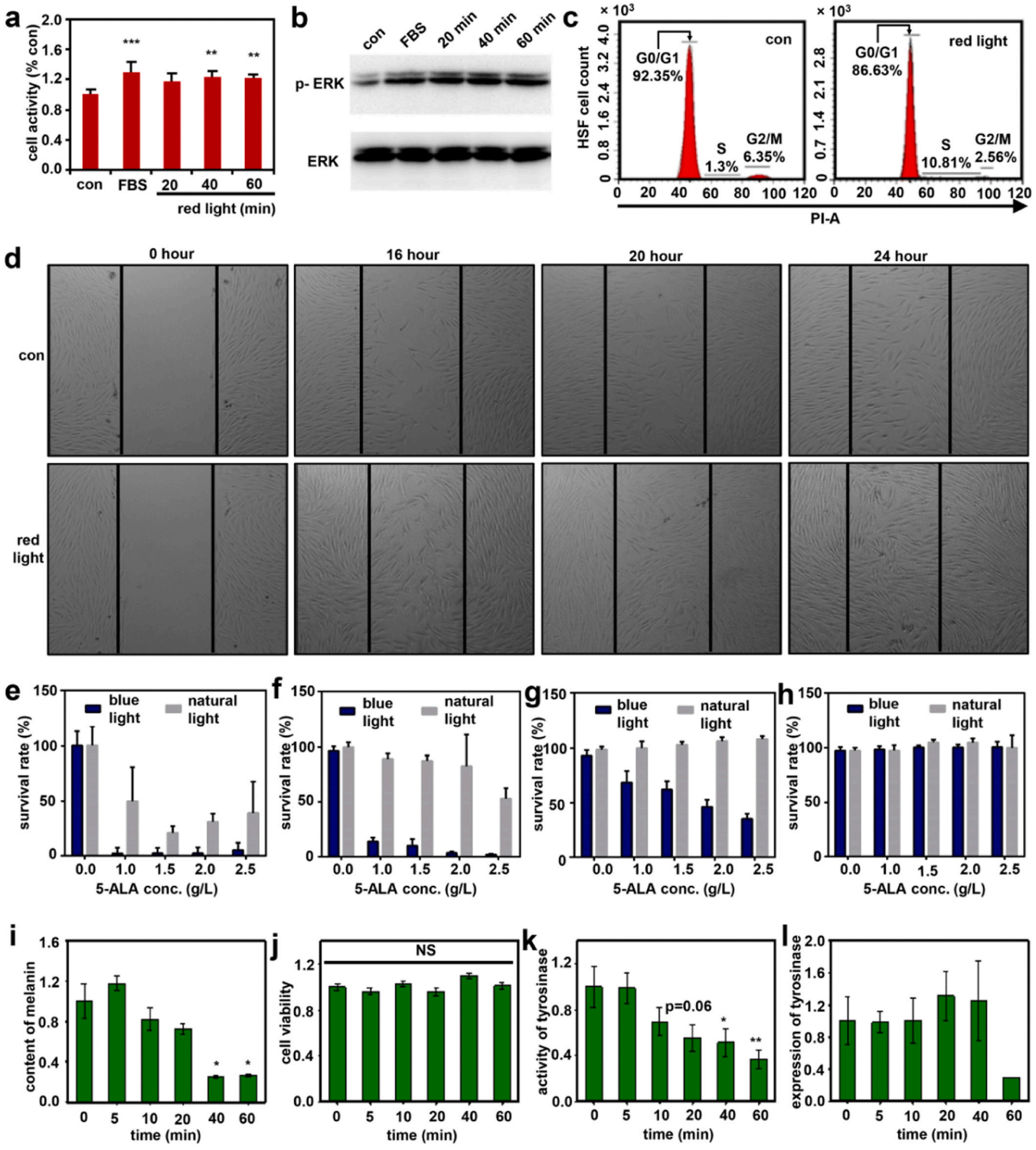

Fig. 4. Effects of tri-color light irradiation by the SEFMPT on skin care. Red light effects: a) activity of the HSFs assessed by the MTT assay; b) ERK phosphorylation level of the HSFs; c) flow cytometry analysis of the HSFs; d) migration of the HSFs following a scratch wound. Blue light effects: e-h) survival rates of *P. acnes* under the initial cfu being 10^4, 10^5, 10^6, and 10^7. Green light effects: i) melanin level assessed by a microplate reader; j) viability of melanocytes (NS: no significant difference); data represented as mean ± SEM ($n = 10$; *P<0.05, **P<0.01 and vs control cells); k) activity of tyrosinase; l) expression of tyrosinase.

mechanical stretchability, low electrical resistance/heat generation, and integration of photodynamic functions are simultaneously achieved by an unusual elaborated design of the island-bridge mesh structure with TMOIC serpentine interconnects that consist of layers of Cu and PI as well as a new PSSP encapsulation technique. The comprehensive design, fabrication, analyses, and tests have been conducted, by which the extraordinary mechanical, thermal and electrical robustness as well as favorable skin care effects of the SEFMPT are confirmed. The present electronic device has great potential for promising applications of stretchable and wearable electronics in the field of photodynamic skin care.

4. Experimental section

Resistance design and simulation of the interconnects: In order to ensure relatively uniform irradiation, the current flow was designed to reduce by 10% at most from the connection port to the far end around the nose tip. The equivalent resistance of the red lights from the tri-color LEDs of type 1516 was the minimum among the three lights when the input current was 9 mA according to the volt-ampere characteristics (Figure S4b, Supporting Information), which was around 222 Ω (~ 2 V / 9 mA). Therefore, the red lights were taken to calculate the resistance of a single bridge as a conservative estimate. According to the volt-ampere characteristics of the red lights, the requirement of 10% decrease of the current corresponded to 5.77 mV decrease of the voltage when the input current was 9 mA with the slope of the volt-ampere curve being 0.0064, which indicated that the resistance of the interconnects between the connection port and the far end should be less than 0.64 Ω, which was contributed by 17 islands and bridges. Therefore, the resistance of a single island and bridge should be less than 37.65 mΩ. The resistance of a single island was estimated to be 4.375 mΩ, we thus obtained the maximum resistance of a single bridge to be 33.275 mΩ, which ensured relatively uniform irradiation. To validate the above resistance design, the numerical simulation by the COMSOL software was conducted for two units of the horizontal and vertical serpentine interconnects (Figure S5, Supporting Information), which gave 33.0 and 30.8 mV voltages under 1 A current, thus yielding 33.0 and 30.8 mΩ resistances, respectively.

Finite element analysis: The FEA was conducted in Abaqus, a widely accepted commercial software, where the compliant elastomeric substrates, including the elastic adhesive (C10=0.00805369, C01=0.00201342, and D1=2) and silicone (C10=0.134228, C01=0.033557, and D1=0.12), were treated as hyper-elastic materials that were described by the Mooney-Rivlin model. PI and Cu were treated as linear elastic and ideal elastic plastic materials, respectively. The Young's modulus, Poisson's ratio of PI are 2.5 GPa and 0.34, respectively. The Young's modulus, Poisson's ratio, and yield stress of Cu are 124 GPa, 0.34, and 372 MPa, respectively. The hexahedron elements C3D8R/C3D6 were adopted for the substrates, and the shell element S4R was adopted for PI and Cu.

Cell proliferation by the SEFMPT: HSFs were obtained from GaiNing Biological (Shanghai, China). HSF cells were plated to 100 mm cell culture plates (Corning, NY) and grown to approximately 75% confluence for 3 more passages in Dulbecco's modified Eagle's medium (DMEM, life Technologies, Inc., NY) containing 10% fetal bovine serum (FBS), then trans-plated into 96-well or 6-well plates for further experiments. Before irradiation with the red light, HSFs were seeded on 96-well microplates for 12 h followed by 24 h serum deprivation. The input current of LEDs was kept at 3.5 A, and the irradiation time was 20, 40, and 60 min, respectively. The irradiation distance was 1.5 cm. Cell activity was assessed by the MTT assay after 24 h. HSFs seeded on 6-well plates were irradiated and then dissolved for western blot assay to analyze the ERK phosphorylation level. HSF cell cycle was analyzed by flow cytometry analysis.

Scratch wound healing assays: For the cell migration assays, HSFs were seeded on 6-well plates in DMEM medium with 10% FBS. The scratch was conducted with 200 μl yellow beveled tips and FBS-deprived DMEM was changed when the plate was 70% covered. The red-light irradiation from the SEFMPT was conducted for 20, 40, and 60 min, and the cells were then cultured for another 24 h. The migrated cells were observed with microscope in starch area.

Inhibition of P. acnes growth by the blue light: *P. acnes* was grown on Wilkins-Chalgren Anaerobe agar from Oxoid Ltd. Irradiation tests were carried out when bacteria were grown in Wilkins-Chalgren Anaerobe Broth with different concentrations of 5-ALA. Assessment of the inhibitory effect of 5-ALA photodynamic therapy on *P. acnes* was carried out as described by the literature [13]. *P. acnes* was transferred from seed culture into the Wilkins-Chalgren Anaerobe agar plates and streaked on the plates for isolation of single colonies. These plates were incubated under anaerobic conditions in an anaerobic jar at 37°C for three days. The jar contained Aaero Gen sachets from Oxoid to maintain anaerobic conditions suitable for *P. acnes*. Single colonies were transferred into the Wilkins-Chalgren Anaerobe Broth and grown anaerobically in the dark for 48 h. The culture was diluted by fresh broth to give an optical density reading (OD 600 nm) of 1.0 and gave approximately 10^8 cfu/mL. Then the culture was serially diluted using fresh broth medium and given approximately 10^7, 10^6, 10^5, and 10^4 cfu/mL cultures. 5-ALA was added to each diluted culture at the final concentration of 0.0, 1.0, 1.5, 2.0, and 2.5 g/L. 200 μL culture was applied to each well of 96-well culture plates. In each 96-well plate, the first and last two lines were assigned as controls and the five lines were assigned as treatment for each diluted culture. The 96-well culture plates with different treatments were incubated at 37°C in the dark for 20 min, then were exposed to the natural light (as the controls) or blue light for 40 min. After taking out 150 μL of culture, each well was refilled with 150 μL fresh broth. After 16 h of incubation, bacterial growth was measured by monitoring the absorbance at 600 nm wavelength in a microplate reader (BioTek, Vermont, USA). Relative survival was calculated by the bacteria concentration ratio of the treatment culture to the control culture without 5-ALA.

Inhibition of melanin synthesis by green light: Melanocyte (PIG-1) was purchased from BeiNa culture collection (Beijing, China) and cultured as HSF cell as described previously. The melanocytes were seeded on 96-well microplates for 12 h, followed by 24 h serum deprivation. The input current of the SEFMPT was kept at 3.5 A, and the irradiation time was 0, 5, 10, 20, 40, and 60 min, respectively. The irradiation distance was 1.5 cm. Cell activity was assessed by the MTT assay after 24 h irradiation. The melanin was extracted from melanocytes, and the content of melanin was reflected by absorption at 450 nm with Synergy H1 Hybrid Multi-Mode Reader (BioTek, Vermont) [45]. For the activity of tyrosinase detection, after 4 h irradiation, melanocytes were lysed and incubated with L-dopa for 10 sec then the absorption at 475 nm was tested. The relative expression of tyrosinase in melanocytes was measured by QPCR after 12 h irradiation.

CRediT authorship contribution statement

Yewang Su: Writing – review & editing, Supervision, Resources, Project administration, Methodology, Conceptualization. **Guangping Gong:** Software. **Ya Yang:** Resources. **Guodong Liu:** Investigation. **Xiaoxiao Jiang:** Writing – review & editing, Writing – original draft, Validation, Software, Methodology, Investigation, Formal analysis, Data curation, Conceptualization. **Qinlan Li:** Software. **Lijuan Zhang:** Writing – review & editing, Writing – original draft, Visualization, Validation, Software, Methodology, Formal analysis, Data curation, Conceptualization. **Mingqi Huang:** Software. **Kun Zhu:** Visualization. **Yuqun Lan:** Writing – review & editing, Software, Investigation. **Yang Zhao:** Visualization. **Shuang Li:** Writing – review & editing, Writing – original draft, Visualization, Validation, Software, Methodology, Investigation, Formal analysis, Conceptualization. **Li Duan:** Software. **Haiying Yu:** Software. **Liang Guo:** Visualization. **Hao Liu:** Software. **Yuli Chen:** Software. **Rui Li:** Supervision, Software. **Juyao Li:** Investigation. **Bo Wang:** Resources. **Maoyi Zhang:** Investigation. **Aochen Wang:** Visualization, Software.

Declaration of Competing Interest

The authors declare that they have no known competing financial interests or personal relationships that could have appeared to influence the work reported in this paper.

Data Availability

Data will be made available on request.

Acknowledgements

The authors gratefully acknowledge the support from the National Natural Science Foundation of China (grants 12172359 and 12022209). Y.S. acknowledges the support from Key Research Program of Frontier Sciences of the Chinese Academy of Sciences (ZDBS-LY-JSC014) and CAS Interdisciplinary Innovation Team (JCTD-2020-03).

Appendix A. Supporting information

Supplementary data associated with this article can be found in the online version at doi:10.1016/j.nanoen.2024.109407.

References

[1] J.A. Rogers, T. Someya, Y. Huang, Science *327* (2010) 1603.
[2] D.Y. Khang, H.Q. Jiang, Y. Huang, J.A. Rogers, Science *311* (2006) 208.
[3] M.H.C. De Vasconcelos Catão, C.F.W. Nonaka, R.L.C. De Albuquerque, P.M. Bento, R. De Oliveira Costa, Lasers Med. Sci. *30* (2015) 421.
[4] Y. Jiang, A.W. Leung, H. Hua, X. Rao, C. Xu, Int. J. Photo *2014* (2014) 637601.
[5] Y. Dong, G. Zhou, J. Chen, L. Shen, Z. Jianxin, Q. Xu, Y. Zhu, Photo Photodyn. Ther. *13* (2016) 188.
[6] M. Asnaashari, H. Ashraf, A. Rahmati, N. Amini, Photo Photodyn. Ther. *17* (2017) 226.
[7] D.-H. Kim, J. Song, W.M. Choi, H.-S. Kim, R.-H. Kim, Z. Liu, Y.Y. Huang, K.-C. Hwang, Y. Zhang, J.A. Rogers, Proc. Natl. Acad. Sci. *105* (2008) 18675.
[8] H. Chung, T. Dai, S.K. Sharma, Y.-Y. Huang, J.D. Carroll, M.R. Hamblin, Ann. Biomed. Eng. *40* (2012) 516.
[9] P.C.L. Silveira, K.B. Ferreira, F.R. Da Rocha, B.L.S. Pieri, G.S. Pedroso, C.T. De Souza, R.T. Nesi, R.A. Pinho, Inflammation *39* (2016) 1395.
[10] N. Zheng, M. Zhou, Y. He, H. Xu, X. Chen, Z. Duan, L. Yang, R. Zeng, Y. Liu, M. Li, Photo Photodyn. Ther. *40* (2022) 103204.
[11] I. Jung, J. Xiao, V. Malyarchuk, C. Lu, M. Li, Z. Liu, J. Yoon, Y. Huang, J.A. Rogers, Proc. Natl. Acad. Sci. *108* (2011) 1788.
[12] A. Ogata, Y. Hasunuma, E. Kikuchi, T. Ishii, M. Ishizuka, Y. Tokuoka, Photo Photodyn. Ther. *19* (2017) 167.
[13] H. Ashkenazi, Z. Malik, Y. Harth, Y. Nitzan, FEMS Immunol. Med. Microbiol. *35* (2003) 17.
[14] A. Slominski, D.J. Tobin, S. Shibahara, J. Wortsman, Physiol. Rev. *84* (2004) 1155.
[15] M. Hassan, Z. Ashraf, Q. Abbas, H. Raza, S.-Y. Seo, Interdiscip. Sci. Comput. Life Sci. *10* (2018) 68.
[16] M.-H. Jeong, K.-M. Yang, J.-K. Kim, B.-H. Nam, G.-Y. Kim, S.-W. Lee, S.-Y. Seo, W.-S. Jo, Int. J. Mol. Med. *31* (2013) 205.
[17] D.-H. Kim, J.-H. Ahn, W.M. Choi, H.-S. Kim, T.-H. Kim, J. Song, Y.Y. Huang, Z. Liu, C. Lu, J.A. Rogers, Science *320* (2008) 507.
[18] H.C. Ko, M.P. Stoykovich, J. Song, V. Malyarchuk, W.M. Choi, C.-J. Yu, J.B. Geddes Iii, J. Xiao, S. Wang, Y. Huang, J.A. Rogers, Nature *454* (2008) 748.
[19] Y. Wang, Z. Lu, Y. Huang, W. Jia, W. Wang, X. Zhang, C. Chen, Y. Li, C. Yang, G. Jiang, Nanomed *18* (2023) 217.
[20] F. Borgia, M. Coppola, R. Giuffrida, S.P. Cannavò, Photo Photodyn. Ther. *26* (2019) 27.
[21] S.Y. Lee, C.E. You, M.Y. Park, Lasers Surg. Med. *39* (2007) 180.
[22] P. Avci, T.T. Nyame, G.K. Gupta, M. Sadasivam, M.R. Hamblin, Lasers Surg. Med. *45* (2013) 349.
[23] H.G. de Araujo, R.M.V. da Silva, P.M. Canela, N. de, F. Silva, F.C. dos Santos-Filho, O.A. Ronzio, M.G.F. de Carvalho, S.D. Santos-Filho, P.F. Meyer, J. Basic, Appl. Sci. *11* (2015) 389.
[24] M.W. Cheon, T.G. Kim, Y.S. Lee, S.H. Kim, Pers. Ubiquitous Comput. *17* (2013) 1421.
[25] C. Guermonprez, L. Declercq, G. Decaux, J. Grimaud, J. Biophotonics *13* (2020) e202000230.
[26] R.A. Weiss, D.H. McDaniel, R.G. Geronemus, M.A. Weiss, Lasers Surg. Med. *36* (2005) 85.
[27] G.K. Keshri, A. Yadav, S. Verma, B. Kumar, A. Gupta, Lasers Surg. Med. *52* (2020) 424.
[28] S. Xu, Y. Zhang, J. Cho, J. Lee, X. Huang, L. Jia, J.A. Fan, Y. Su, J. Su, H. Zhang, H. Cheng, B. Lu, C. Yu, C. Chuang, T. Kim, T. Song, K. Shigeta, S. Kang, C. Dagdeviren, I. Petrov, P.V. Braun, Y. Huang, U. Paik, J.A. Rogers, Nat. Commun. *4* (2013) 1543.
[29] L. Longo, R. Lubart, H. Friedman, R. Lavie, in (Eds.: L. Longo, A. G. Hofstetter, M.-L. Pascu, W. R. A. Waidelich), 2004, pp. 158–164.
[30] Y. Taniguchi, T. Ohshiro, T. Ohshiro, K. Sasaki, S. Fujii, LASER Ther. *16* (2007) 137.
[31] A. Baker, J. Aesthetic Nurs. *5* (2016) 478.
[32] H. Tao, M.A. Brenckle, M. Yang, J. Zhang, M. Liu, S.M. Siebert, R.D. Averitt, M. S. Mannoor, M.C. McAlpine, J.A. Rogers, D.L. Kaplan, F.G. Omenetto, Adv. Mater. *24* (2012) 1067.
[33] J.-W. Jeong, W.-H. Yeo, A. Akhtar, J.J.S. Norton, Y.-J. Kwack, S. Li, S.-Y. Jung, Y. Su, W. Lee, J. Xia, H. Cheng, Y. Huang, W.-S. Choi, T. Bretl, J.A. Rogers, Adv. Mater. *25* (2013) 6839.
[34] X. Yan, H. Li, W. Zheng, X. Su, Anal. Chem. *87* (2015) 8904.
[35] N. Lu, X. Wang, Z. Suo, J. Vlassak, Appl. Phys. Lett. *91* (2007) 221909.
[36] Y. Xiang, T. Li, Z. Suo, J.J. Vlassak, Appl. Phys. Lett. *87* (2005) 161910.
[37] T. Li, Z. Suo, Int. J. Solids Struct. *44* (2007) 1696.
[38] T. Li, Z. Huang, Z. Suo, S.P. Lacour, S. Wagner, Appl. Phys. Lett. *85* (2004) 3435.
[39] N. Lu, Z. Suo, J.J. Vlassak, Acta Mater. *58* (2010) 1679.
[40] X. Cheng, F. Zhang, R. Bo, Z. Shen, W. Pang, T. Jin, H. Song, Z. Xue, Y. Zhang, Adv. Mater. *33* (2021) 2102684.
[41] D.-H. Kim, N. Lu, R. Ma, Y.-S. Kim, R.-H. Kim, S. Wang, J. Wu, S.M. Won, H. Tao, A. Islam, K.J. Yu, T. Kim, R. Chowdhury, M. Ying, L. Xu, M. Li, H.-J. Chung, H. Keum, M. McCormick, P. Liu, Y.-W. Zhang, F.G. Omenetto, Y. Huang, T. Coleman, J.A. Rogers, Science *333* (2011) 838.
[42] Y. Su, X. Ping, K.J. Yu, J.W. Lee, J.A. Fan, B. Wang, M. Li, R. Li, D.V. Harburg, Y. Huang, C. Yu, S. Mao, J. Shim, Q. Yang, P. Lee, A. Armonas, K. Choi, Y. Yang, U. Paik, T. Chang, T.J. Dawidczyk, Y. Huang, S. Wang, J.A. Rogers, Adv. Mater. *29* (2017) 1604989.
[43] M. Zhuang, L. Yin, Y. Wang, Y. Bai, J. Zhan, C. Hou, L. Yin, Z. Xu, X. Tan, Y. Huang, Research *2021* (2021) 9759601.
[44] A.J. Singer, R.A.F. Clark, N. Engl. J. Med *341* (1999) 738.
[45] J.M. Naeyaert, M. Eller, P.R. Gordon, H.-Y. Park, B.A. Gilchrest, Br. J. Dermatol. *125* (1991) 297.